INTERNATIONAL JOURNAL FOR NUMERICAL METHODS IN FLUIDS
Int. J. Numer. Meth. Fluids 2002; **40**:927–949 (DOI: 10.1002/fld.383)

Feedback control of the Rayleigh–Bénard convection by means of mode reduction

H. M. Park* and W. J. Lee

Department of Chemical Engineering, Sogang University, C.P.O. Box 442, Seoul 100-611, Korea

SUMMARY

An optimal feedback control is synthesized for the Rayleigh–Bénard convection by means of empirical reduction of modes. The Boussinesq equation is reduced to a minimal set of ordinary differential equations by using the Karhunen–Loève Galerkin procedure. The state feedback control synthesis, that drives the intensity of convection to a preset trajectory by adjusting heat flux at the bottom of the system, is constructed using this low-dimensional dynamic model by first performing an extended Kalman filter estimate of the velocity and temperature fields and then developing the optimal feedback law by means of the linear regulator theory. The present technique allows for the practical implementation of modern control concepts to the natural convection and is found to yield satisfactory results. Copyright © 2002 John Wiley & Sons, Ltd.

KEY WORDS: feedback control; Rayleigh–Bénard convection; Karhunen–Loève Galerkin procedure

1. INTRODUCTION

The Rayleigh–Bénard convection is a classic problem of natural convection for a horizontal fluid layer heated from below, and is a first approach to highly complex thermal convection processes in industry. The dimensionless number corresponding to the temperature gradient in the system is the Rayleigh number, and convection sets in only when the Rayleigh number is above the critical value. The determination of the critical Rayleigh number and how the intensity of the convection varies with the Rayleigh number are well documented in Chandrasekhar [1] and Drazin and Reid [2]. In many industrial applications it may be desirable to return the pattern of convection to a preset one or to make it follow a prescribed trajectory promptly by exploiting the velocity or temperature measurements when there are initial deviation or disturbance. These are typical feedback control problems [3]. In the present investigation, we develop an applicable method of optimal state feedback control for the Rayleigh–Bénard convection, that enforces the system to return to the preset state promptly by adjusting the heat flux at the bottom of the domain. The feedback controller determines the control inputs of the

* Correspondence to: H. M. Park, Department of Chemical Engineering, Sogang University, C.P.O. Box 442, Seoul 100-611, Korea.

Received 23 October 2000
Revised 3 May 2002

system, i.e. the spatial distribution of heat flux at the bottom, on the basis of the observations of the present velocity and temperature fields, thus reducing the effect of external disturbances and uncertainties. In reality, we can measure the velocity and temperature only at a limited number of locations and the complete state, needed in the state feedback control scheme, must be estimated from these partial observations by means of an identification scheme. Thus, the design of an optimal feedback control is divided into two parts: the linear quadratic regulator (LQR) and the minimum variance estimator (Kalman filter). LQR provides an optimal control law in terms of the present state of the system [3]. The Kalman filter provides an optimal estimate of the present state based on the partial measurements available [4]. But the straightforward implementation of the above scheme on the governing equation of natural convection, the Boussinesq set, encounters a serious difficulty. The tremendous requirement of computer time and memory to solve the covariance equations in the Kalman filter and LQR renders this scheme virtually useless. The only way of circumventing this difficulty is to devise a reduced order model or a low-dimensional dynamic model that simulates the system faithfully. An appropriate technique for this purpose is the Karhunen–Loève Galerkin procedure.

The Karhunen–Loève Galerkin procedure [5, 6] is a type of Galerkin method that employs the empirical eigenfunctions of the Karhunen–Loève decomposition [7] as basis functions. The Karhunen–Loève decomposition had been devised as a rational technique enabling a stochastic field to be represented with a minimum degree of freedom. If the Karhunen–Loève decomposition is applied to a given stochastic field, we get a set of empirical eigenfunctions. When we want to reproduce the same stochastic field, it can be done with a minimum degree of freedom by using these empirical eigenfunctions. Recently, the applicability of the Karhunen–Loève decomposition had been extended to the analysis of non-stationary, non-homogeneous deterministic as well as stochastic fields to allow the derivation of rigorous reduced order models that stimulate the given systems almost exactly [5, 6]. This extension of the original Karhunen–Loève decomposition is called the Karhunen–Loève Galerkin procedure. By employing the empirical eigenfunctions of the Karhunen–Loève decomposition as basis functions, the Karhunen–Loève Galerkin procedure can *a priori* limit the function space considered to the smallest subspace that is sufficient to describe the observed solutions, and consequently reduce the given partial differential equations to a minimal set of ordinary differential equations. In Park and Lee [8], the Karhunen–Loève Galerkin procedure is employed to solve an open-loop optimal control problem of the Navier–Stokes equation. But the open-loop control is generally not useful for practical applications, and a more practical and useful control scheme is obtained by introducing the concept of feedback which allows to determine the control inputs of the system on the basis of the observations of the present state. The use of feedback is, in particular, important when the dynamics of the system is only partially known due to the presence of uncertainty and external disturbances. In the present investigation, we employ the Karhunen–Loève Galerkin procedure to construct a feedback control for the Rayleigh–Bénard convection. The details of the Karhunen–Loève Galerkin procedure are explained in our previous works [5, 6, 8].

2. GOVERNING EQUATIONS

We consider a two-dimensional rectangular cavity filled with a Boussinesq fluid. Due to the heat flux imposed at the bottom boundary, natural convection is induced in the domain. Our

aim is to drive the pattern of convection to a preset trajectory by adjusting heat flux at the bottom of the system based on the velocity and temperature measurements at selected locations in the system domain. Although the natural convection is three-dimensional in many practical situations, the present two-dimensional example facilitates the demonstration of the Karhunen–Loève Galerkin procedure as applied to the feedback control synthesis. Extension of the subsequent analysis to three-dimensional problems is trivial. The governing equations for the system may be written in dimensionless variables as follows:

$$\nabla \cdot \mathbf{v} = 0 \tag{1}$$

$$\frac{\partial \mathbf{v}}{\partial t} + \mathbf{v} \cdot \nabla \mathbf{v} = -\nabla P + Pr\, \nabla^2 \mathbf{v} + R\, Pr\, T\mathbf{j} \tag{2}$$

$$\frac{\partial T}{\partial t} + \mathbf{v} \cdot \nabla T = \nabla^2 T \tag{3}$$

with the relevant initial and boundary conditions

$$t = 0, \quad \mathbf{v} = \mathbf{v}_0, \quad T = T_0 \tag{4}$$

$$x = \pm 1, \quad \mathbf{v} = 0, \quad \frac{\partial T}{\partial x} = 0 \tag{5}$$

$$y = 1, \quad \mathbf{v} = 0, \quad T = 0 \tag{6}$$

$$y = -1, \quad \mathbf{v} = 0, \quad \frac{\partial T}{\partial y} = -\frac{d_y}{k(T_{\mathrm{H}}^* - T_{\mathrm{C}}^*)}\, q(x,t) \tag{7}$$

where $\mathbf{v}_0$ and T_0 are the initial velocity and temperature fields. The dimensionless variables are defined by the following relations, where the superscript asterisk denotes dimensional quantities

$$x = \frac{x^*}{d_x}, \quad y = \frac{y^*}{d_y}, \quad t = \frac{\kappa t^*}{d_y^2}, \quad \mathbf{v} = \frac{d_y \mathbf{v}^*}{\kappa}, \quad T = \frac{T^* - T_{\mathrm{C}}^*}{T_{\mathrm{H}}^* - T_{\mathrm{C}}^*}, \quad P' = \frac{d_y^2 P^*}{\rho \kappa^2} \tag{8}$$

where T_{C}^* is the dimensional temperature at the top boundary, T_{H}^* is the nominal bottom temperature which is determined by the heat flux at the bottom or the Rayleigh number, κ is the thermal diffusivity, k is the thermal conductivity, d_x is the half-width and d_y is the half-depth of the cavity. The modified pressure P is given by

$$P = P' - (T_{\mathrm{C}}^* - T_{\mathrm{ref}}^*)\, \frac{d_y^3}{\kappa^2}\, \alpha g y \tag{9}$$

where T_{ref}^* is the reference temperature defined by

$$T_{\mathrm{ref}}^* = \tfrac{1}{2}(T_{\mathrm{H}}^* + T_{\mathrm{C}}^*) \tag{10}$$

The dimensionless group R is the Rayleigh number and Pr is the Prandtl number defined as follows:

$$R = \alpha g \frac{(T_H^* - T_C^*)d_y^3}{\kappa v}, \quad Pr = \frac{v}{\kappa} \tag{11}$$

where α is the thermal expansion coefficient, v is the kinematic viscosity and g is the gravitational constant. Combining Equations (7)–(11), we may rewrite the Rayleigh number in terms of the average heat flux q_0

$$R = \alpha g \frac{2d_y^4 q_0}{k\kappa v} \tag{12}$$

where

$$q_0 \equiv \frac{1}{2} \int_{x=-1}^{1} q(x,t)\,\mathrm{d}x \tag{13}$$

The set of Equations (1)–(3) is solved by using the Chebyshev pseudospectral method employing (40×20) grids, which is tested and found to be sufficient to resolve the fields. The details of the Chebyshev pseudospectral method as applied to the Boussinesq equation are explained in Park and Chung [9].

3. KARHUNEN–LOÈVE GALERKIN PROCEDURE

The Karhunen–Loève Galerkin procedure consists of the following three basic steps: preparation of various velocity and temperature fields, extraction of empirical eigenfunctions from these fields, construction of the low-dimensional dynamic model using empirical eigenfunctions.

3.1. Preparation of velocity and temperature fields

Since the empirical eigenfunctions, which constitute the space for the low-dimensional dynamic model, are expressed linearly in terms of velocity and temperature fields [5, 6], the velocity and temperature fields must be prepared such that they fully characterize the system dynamics. We assume that the heat flux function $q(x,t)$ can be expressed as

$$q(x,t) = \sum_{n=1}^{N} A(t) \cos\left[\frac{(n-1)\pi(x+1)}{2}\right] \quad (n = 1,2,\ldots,N) \tag{14}$$

Next, we solve the system governing equations, Equations (1)–(3), with $q(x,t) = A(t)\cos[(n-1)\pi(x+1)/2]$ and record the velocity and temperature fields at a regular time interval until $t = t_f$. These recordings of the velocity and temperature fields are used later in the Karhunen–Loève decomposition to extract the empirical eigenfunctions. With $(A,n) = (15,1)$, we integrate Equations (1)–(3) from $t = 0$ until $t = t_f(= 0.5)$ to obtain a hundred velocity and a hundred temperature fields, respectively. Repeating this procedure with $(A,n) = (15,2)$, $(15,3),\ldots,(15,10),(-15,1),\ldots,(-15,10)$, we obtain two thousand velocity and two thousand temperature fields. To characterize the dynamic behaviour of the system better, the set of

these fields are reinforced by adding another one thousand velocity and one thousand temperature fields which are obtained by solving Equations (1)–(3) with $A(t) = 15\sin(n\pi t/t_f)$ and $n = 1, 2, \ldots, 10$, respectively. In this way we obtain a set of three thousand velocity fields and a set of three thousand temperature fields, from which the velocity and temperature empirical eigenfunctions are to be extracted. The detailed rationale behind the above procedure can be found in Park and Cho [5] and Park and Lee [6].

3.2. Determination of empirical eigenfunctions

As explained in Park and Cho [5] and Park and Lee [6], the empirical eigenfunctions of the Karhunen–Loève decompositions are obtained by solving the following integral equations.

$$\int \mathbf{K}^{(\mathbf{v})}(\mathbf{x}, \mathbf{x}')\boldsymbol{\phi}(\mathbf{x}')\,\mathrm{d}\mathbf{x}' = \lambda^M \boldsymbol{\phi}(\mathbf{x}) \tag{15}$$

$$\int K^{(T)}(\mathbf{x}, \mathbf{x}')\varphi(\mathbf{x}')\,\mathrm{d}\mathbf{x}' = \lambda^T \varphi(\mathbf{x}) \tag{16}$$

where $\boldsymbol{\phi}(\mathbf{x})$ and $\varphi(\mathbf{x})$ are the velocity empirical eigenfunction and the temperature empirical eigenfunction, respectively, and $\mathbf{K}^{(\mathbf{v})}$ and $K^{(T)}$ are the corresponding two-point correlation functions defined as

$$\mathbf{K}^{(\mathbf{v})}(\mathbf{x}, \mathbf{x}') = \frac{1}{M}\sum_{j=1}^{M} \mathbf{v}^{(j)}(\mathbf{x})\mathbf{v}^{(j)}(\mathbf{x}') \tag{17}$$

$$K^{(T)}(\mathbf{x}, \mathbf{x}') = \frac{1}{M}\sum_{j=1}^{M} T^{(j)}(\mathbf{x})T^{(j)}(\mathbf{x}') \tag{18}$$

Here $\mathbf{v}^{(j)}$ is the jth velocity field, $T^{(j)}$ is the jth temperature field and $M(=3000)$ is the total number of fields which are obtained as explained in Section 3.1 and adopted in the Karhunen–Loève decomposition. The integral equations, Equations (15) and (16), can be solved by using the Schmidt–Hilbert technique [5, 6, 10], where the eigenfunctions are represented as linear combinations of the corresponding fields. After solving Equations (15) and (16), we get the velocity and temperature empirical eigenfunctions in the order of their importance in characterizing the system. Figures 1(a) and (b) plot the accumulated normalized eigenvalues, $\Sigma\lambda_i^M$ and $\Sigma\lambda_i^T$, versus the number of velocity and temperature eigenfunctions. They show that the convergence rates of the velocity eigenvalues λ_i^M and the temperature eigenvalues λ_i^T are very rapid.

3.3. Construction of low-dimensional dynamic model

The Boussinesq set, Equations (1)–(3), is reduced to a set of ordinary differential equations by assuming

$$\mathbf{v} = \sum_{n=1}^{NM} a_n(t)\boldsymbol{\phi}_{(n)}(\mathbf{x}) \tag{19}$$

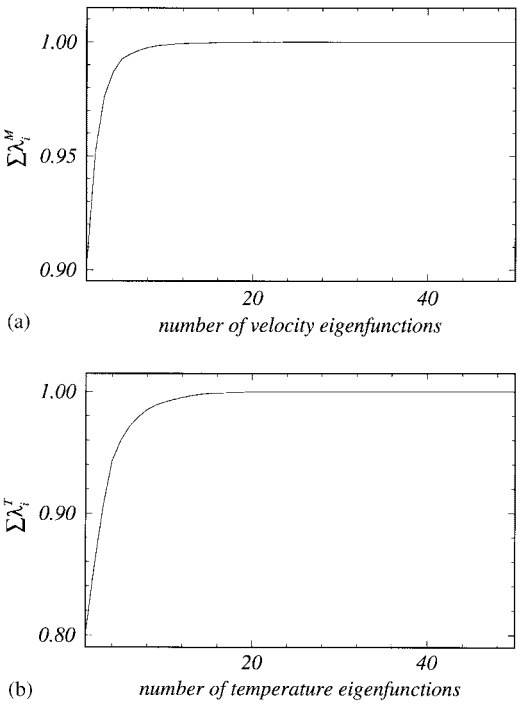

Figure 1. Accumulated normalized eigenvalues vs number of eigenfunctions: (a) velocity eigenvalues λ^M, and (b) temperature eigenvalues λ^T.

$$T = \sum_{n=1}^{NT} b_n(t)\varphi_{(n)}(\mathbf{x}) \tag{20}$$

where $\boldsymbol{\phi}_{(n)}$ is the nth velocity eigenfunction and $\varphi_{(n)}$ is the nth temperature eigenfunction. Substituting Equations (19) and (20) into Equations (1)–(3) and applying the Galerkin principle which enforces the residual to be orthogonal to each of the basis functions, Equations (1)–(3) with the relevant boundary conditions are reduced to the following sets of ordinary differential equations

$$M_j \frac{\mathrm{d}a_j}{\mathrm{d}t} + \sum_{l=1}^{NM}\sum_{m=1}^{NM} a_l a_m Q_{jlm} + Pr \sum_{l=1}^{NM} H_{jl} a_l - R\,Pr \sum_{l=1}^{NT} b_l S_{jl} = 0 \tag{21}$$

$$N_j \frac{\mathrm{d}b_j}{\mathrm{d}t} + \sum_{l=1}^{NM}\sum_{m=1}^{NT} a_l b_m R_{jlm} + \sum_{l=1}^{NT} L_{jl} b_l = \frac{d_y}{k(T_{\mathrm{H}}^* - T_{\mathrm{C}}^*)} \int_{x=-1}^{1} q(x,t)\varphi_j(x, y=-1)\,\mathrm{d}x \tag{22}$$

In the above equations

$$M_j \equiv \int_\Omega \boldsymbol{\phi}_{(j)} \cdot \boldsymbol{\phi}_{(j)}\,\mathrm{d}\Omega, \quad Q_{jlm} \equiv \int_\Omega \boldsymbol{\phi}_{(j)} \cdot (\boldsymbol{\phi}_{(l)} \cdot \nabla\boldsymbol{\phi}_{(m)})\,\mathrm{d}\Omega$$

$$H_{jl} \equiv \int_\Omega (\nabla \boldsymbol{\phi}_{(j)}) : (\nabla \boldsymbol{\phi}_{(l)})^{\mathrm{T}} \, \mathrm{d}\Omega, \quad S_{jl} \equiv \int_\Omega \varphi_{(l)} \phi^v_{(j)} \, \mathrm{d}\Omega$$

$$N_j \equiv \int_\Omega \varphi^2_{(j)} \, \mathrm{d}\Omega, \quad R_{jlm} \equiv \int_\Omega (\boldsymbol{\phi}_{(l)} \cdot \nabla \varphi_{(m)}) \varphi_{(j)} \, \mathrm{d}\Omega \tag{23}$$

$$L_{jl} \equiv \int_\Omega \nabla \varphi_{(l)} \cdot \nabla \varphi_{(j)} \, \mathrm{d}\Omega$$

where $\phi^u_{(j)}$ and $\phi^v_{(j)}$ are the x- and y-component of the jth velocity eigenfunction and Ω is the system domain. The accuracy of the low-dimensional dynamic model improves as the number of empirical eigenfunctions employed (i.e. NM and NT) increases up to the optimal number. But further increase of number of eigenfunctions beyond the optimal number does not always improve the accuracy because the empirical eigenfunctions with very small eigenvalues are usually contaminated with round-off errors [5, 6, 8]. A convenient guideline for the determination of the optimal number is that one minus the sum of the normalized eigenvalues of the eigenfunctions employed in the low-dimensional model should be approximately the same as the inherent numerical error, i.e. the sum of the truncation and round-off errors. The optimal numbers of the velocity and temperature eigenfunctions for the set of Equations (21) and (22) are found to be $NM = 19$ and $NT = 32$. Employing these numbers of empirical eigenfunctions, the relative error of the low-dimensional dynamic model with respect to the exact numerical solution of the Boussinesq equation is found to be less than 2% for various heat flux $q(x, t)$.

4. FEEDBACK CONTROL SYNTHESIS

The optimal state feedback controller determines the control inputs of the system, i.e. the spatial distribution of heat flux at the bottom, on the basis of the partial observations of the present velocity and temperature fields. Since the LQR theory requires the complete state of the system to determine the control inputs, it is necessary to reconstruct the complete state of the system from the partial measurements using an estimator such as the Kalman filter. Therefore, the two basic steps in the feedback control synthesis is the state identification and the LQR. In the sequel, we address the state identification and the construction of feedback control for the following two problems.

Problem A: We want to determine a spatial distribution of heat flux at each moment, $q(x, t)$, that drives the system to a preset constant state promptly in an optimal manner, based on the velocity and temperature measurements at certain locations. Namely,

Minimize:

$$J = \frac{1}{2} \int_0^{t_\mathrm{f}} \int_\Omega (\mathbf{v}(\mathbf{x}, t) - \mathbf{v}_e(\mathbf{x}))^2 + \omega_T (T(\mathbf{x}, t) - T_e(\mathbf{x}))^2 \, \mathrm{d}\Omega \, \mathrm{d}t$$

$$+ \frac{\varepsilon}{2} \int_0^{t_\mathrm{f}} \int_{x=-1}^{1} (q(x, t) - q_e(x))^2 \, \mathrm{d}x \, \mathrm{d}t \tag{24}$$

where $\mathbf{v}_e(\mathbf{x})$ and $T_e(\mathbf{x})$ are the preset velocity and temperature field and ω_T is a weighting factor. The steady velocity and temperature field when $q(x, t) = q_e(x) = 5\cos[(3\pi/2)(x+(2/3))]$

are chosen as $\mathbf{v}_e(\mathbf{x})$ and $T_e(\mathbf{x})$. The present states $\mathbf{v}(\mathbf{x},t)$ and $T(\mathbf{x},t)$ are estimated by means of the Kalman filter based on the velocity and temperature measurements at the selected locations.

Problem B: In this problem, we determine an optimal $q(x,t)$ that enforces the system to follow a prescribed trajectory promptly based on the velocity and temperature measurements at the selected locations. The optimal $q(x,t)$ is determined according to the criterion given by Equation (24). For this problem, $\mathbf{v}_e(\mathbf{x})$ and $T_e(\mathbf{x})$ are the stationary fields when $q(x,t) = 5\cos[(3\pi/2)(x+(2/3))]\sin(2\pi t/t_f)$. The present states $\mathbf{v}(\mathbf{x},t)$ and $T(\mathbf{x},t)$ are determined by the Kalman filter to be derived later.

4.1. State identification

In the present investigation, we employ the extended Kalman filter [4] for the purpose of state identification. We rewrite the low-dimensional dynamic model, Equations (21) and (22), in the following standard form:

$$\frac{\mathrm{d}\mathbf{x}}{\mathrm{d}t} = \mathbf{f} + \mathbf{D}\cdot\mathbf{q} + \boldsymbol{\xi}(t) \tag{25}$$

where

$$\begin{aligned}\mathbf{x} &= (a_1, a_2, \ldots, a_{NM}, b_1, b_2, \ldots, b_{NT})^{\mathrm{T}} \\ &= (x_1, x_2, \ldots, x_{NM+NT})^{\mathrm{T}}\end{aligned} \tag{26}$$

$$\mathbf{f} = \begin{bmatrix} -\sum_{l=1}^{NM}\sum_{m=1}^{NM} a_l a_m \dfrac{Q_{jlm}}{M_j} - Pr\sum_{l=1}^{NM}\dfrac{H_{jl}}{M_j}a_l + R\,Pr\sum_{l=1}^{NT}\dfrac{S_{jl}}{M_j}b_l \\ -\sum_{l=1}^{NM}\sum_{m=1}^{NT} a_l b_m \dfrac{R_{jlm}}{N_j} - \sum_{l=1}^{NT}\dfrac{L_{jl}}{N_j}b_l \end{bmatrix} \tag{27}$$

$$\mathbf{D} = \frac{d_y}{k(T_{\mathrm{H}}^* - T_{\mathrm{C}}^*)} \begin{bmatrix} \mathbf{O} \\ \hline \dfrac{Z_{11}}{N_1} & \dfrac{Z_{21}}{N_1} & \cdots & \dfrac{Z_{N1}}{N_1} \\ \dfrac{Z_{12}}{N_2} & \dfrac{Z_{22}}{N_2} & \cdots & \dfrac{Z_{N2}}{N_2} \\ \vdots & & \vdots & \\ \dfrac{Z_{1,NT}}{N_{NT}} & \dfrac{Z_{2,NT}}{N_{NT}} & \cdots & \dfrac{Z_{N,NT}}{N_{NT}} \end{bmatrix} \tag{28}$$

$$\mathbf{q} = (q_1 \quad q_2 \quad \cdots \quad q_N)^{\mathrm{T}} \tag{29}$$

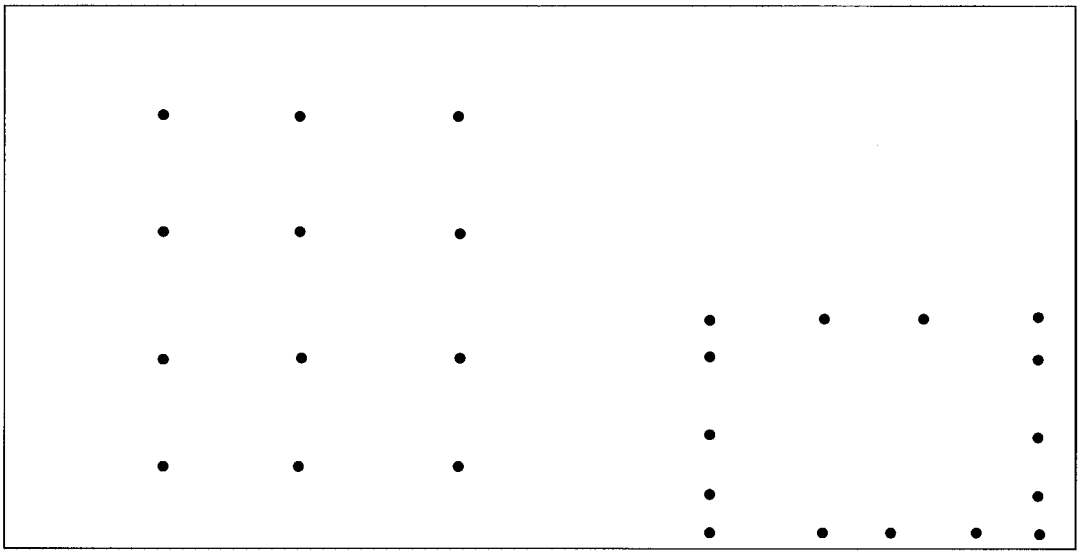

Figure 2. Measurement locations.

and

$$Z_{nj} \equiv \int_{x=-1}^{1} \cos\left[\frac{(n-1)\pi(x+1)}{2}\right] \varphi_j(x, y=-1)\,\mathrm{d}x \tag{30}$$

$$q(x,t) = \sum_{n=1}^{N} q_n(t) \cos\left[\frac{(n-1)\pi(x+1)}{2}\right] \tag{31}$$

In Equation (28), $\mathbf{O}$ is a zero matrix of size (NM,N). The velocity and temperature measurements at the MO locations, depicted in Figure 2, may be represented as follows:

$$\mathbf{v}^*(x_m, y_m, t) = \sum_{j=1}^{NM} a_j \boldsymbol{\phi}_{(j)}(x_m, y_m) \quad (m = 1, 2, \ldots, MO) \tag{32}$$

$$T^*(x_m, y_m, t) = \sum_{j=1}^{NT} b_j \varphi_{(j)}(x_m, y_m) \quad (m = 1, 2, \ldots, MO) \tag{33}$$

The above equation may be rewritten as

$$\mathbf{y} = \mathbf{C}\mathbf{x} + \boldsymbol{\eta} \tag{34}$$

where

$$\mathbf{y} = (u^*(x_1, y_1), \ldots, u^*(x_{MO}, y_{MO}), v^*(x_1, y_1), \ldots, v^*(x_{MO}, y_{MO}),$$
$$T^*(x_1, y_1), \ldots, T^*(x_{MO}, y_{MO}))^{\mathrm{T}} \tag{35}$$

and (u, v) is the components of the velocity vector $\mathbf{v}$. In Equations (25) and (34), $\boldsymbol{\xi}$ is the Gaussian white modelling noise and $\boldsymbol{\eta}$ is the Gaussian white measurement noise. Using Equations (25) and (34), the performance function for the identification of the velocity and temperature fields is expressed as follows:

$$J = \frac{1}{2}[\mathbf{x}(0) - \mathbf{x}_0]^{\mathrm{T}}\mathbf{P}_0^{-1}[\mathbf{x}(0) - \mathbf{x}_0] + \frac{1}{2}\int_0^{t_f}\{[\dot{\mathbf{x}} - \mathbf{f} - \mathbf{D}\cdot\mathbf{q}]^{\mathrm{T}}\mathbf{R}[\dot{\mathbf{x}} - \mathbf{f} - \mathbf{D}\cdot\mathbf{q}]\}\mathrm{d}t + \frac{1}{2}\int_0^{t_f}\{[\mathbf{y} - \mathbf{C}\mathbf{x}]^{\mathrm{T}}\mathbf{Q}[\mathbf{y} - \mathbf{C}\mathbf{x}]\}\,\mathrm{d}t \tag{36}$$

where the weighting matrices $\mathbf{P}_0^{-1}$, $\mathbf{R}$ and $\mathbf{Q}$ can be chosen to reflect the errors in the initial estimate, the model and the measurement device, respectively. The standard procedure to derive the sequential identification equation is as follows [4]. The performance function (36) is minimized using a variational method to yield a two-point boundary value problem. Applying the Riccati transformation to the resulting two-point boundary-value problem, the following Kalman filtering equation is derived

$$\frac{\mathrm{d}\mathbf{x}}{\mathrm{d}t} = \mathbf{f} + \mathbf{D}\cdot\mathbf{q} + \mathbf{P}\mathbf{C}^{\mathrm{T}}\mathbf{Q}[\mathbf{y} - \mathbf{C}\mathbf{x}] \tag{37}$$

$$\frac{\mathrm{d}\mathbf{P}}{\mathrm{d}t} = \mathbf{P}\mathbf{A}^{\mathrm{T}} + \mathbf{A}\mathbf{P}^{\mathrm{T}} + \mathbf{R}^{-1} - \mathbf{P}\mathbf{C}^{\mathrm{T}}\mathbf{Q}\mathbf{C}\mathbf{P} \tag{38}$$

where $\mathbf{P}$ is the error covariance matrix. Because the length of the vector $\mathbf{x}$ is $(NM + NT)$, the covariance matrix $\mathbf{P}$ is of the size $(NM + NT, NM + NT)$ and symmetric. Thus, the number of equations to be solved to obtain $\mathbf{P}$ is $(NM + NT)(NM + NT + 1)/2$. The matrix $\mathbf{A}$ in Equation (38) is the Jacobian matrix evaluated at the previous estimation

$$\mathbf{A} \equiv \frac{\partial \mathbf{f}}{\partial \mathbf{x}} \tag{39}$$

Specifically, its components are given by

$$\frac{\partial f_j}{\partial x_i} = -\sum_{m=1}^{NM} x_m \frac{Q_{jim}}{M_j} - \sum_{l=1}^{NM} x_l \frac{Q_{jli}}{M_j} - \frac{Pr\,H_{ji}}{M_j} \quad (j = 1, 2, \ldots, NM; i = 1, 2, \ldots, NM) \tag{40}$$

$$\frac{\partial f_j}{\partial x_i} = \frac{R\,PrS_{j,i-NM}}{M_j} \quad (j = 1, 2, \ldots, NM; i = NM + 1, \ldots, NM + NT) \tag{41}$$

$$\frac{\partial f_j}{\partial x_i} = -\sum_{m=1}^{NT} x_{NM+m} \frac{R_{j-NM,i,m}}{N_{j-NM}} \quad (j = NM + 1, \ldots, NM + NT; i = 1, 2, \ldots, NM) \tag{42}$$

$$\frac{\partial f_j}{\partial x_i} = -\sum_{l=1}^{NM} x_l \frac{R_{j-NM,l,i-NM}}{N_{j-NM}} - \frac{L_{j-NM,i-NM}}{N_{j-NM}}$$

$$(j = NM+1,\ldots,NM+NT; i = NM+1,\ldots,NM+NT) \tag{43}$$

The initial values of $\mathbf{P}$ and $\mathbf{Q}$ are assumed to be $\mathbf{P} = 0.9\mathbf{I}$ and $\mathbf{Q} = (1/0.0025)\mathbf{I}$, respectively. The model error $\mathbf{R}^{-1}$ is neglected in the present computation. To assess the performance of the Kalman filter, Equations (37) and (38), we consider first the problem A, defined in the previous section, when there is a large error in the initial estimation of the velocity and temperature fields. Figure 3 shows the temporal variations of $\mathbf{v}^2$ and T^2 integrated over the domain when we use the Kalman filter equation (Equations (37), (38)) where the measurements at the selected locations indicated in Figure 2 are employed and when we use the low-dimensional dynamic model (Equation (25)) which do not exploit the measurements, respectively. The velocity and temperature measurements are assumed to have 3% relative error which is Gaussian randomly distributed. It is shown that the Kalman filter predicts the velocity and temperature fields very accurately even though quite inaccurate initial estimation is adopted. Figures 4(a)–4(c) show the velocity and temperature trajectories at selected points, which are indicated at the top of the figure, to reaffirm the performance of the Kalman filter. Figures 5 and 6(a)–6(c) show similar results of the state estimation for the problem B. The Kalman filter is shown to estimate the system state accurately after a very short transient period, even with 3% measurement error.

4.2. Optimal state feedback control

In this section, we consider the combination of feedback control with state estimation. It is based on the separation principle which states that the design of an optimal control problem with measurement and model uncertainty can be treated by first performing a Kalman filter estimate of the states and then developing the optimal control law exploiting the estimated states [3]. The application of the separation principle allows for the practical implementation of feedback control concepts to systems with significant measurement uncertainties. An optimal feedback controller is synthesized by using the linear regulator theory [3]. Our purpose is to regulate the system about an equilibrium or stationary state when we have an initial offset. In other words, we try to return the velocity and temperature fields to a preset constant value or make the fields follow a prescribed trajectory promptly when there are initial deviation or disturbance. The feedback control law may be derived by applying LQR to the low-dimensional model, Equation (25), as follows. The equilibrium or stationary state $\mathbf{x}_e$ satisfies

$$\frac{\mathrm{d}\mathbf{x}_e}{\mathrm{d}t} = \mathbf{f}(\mathbf{x}_e) + \mathbf{D}\cdot\mathbf{q}_e \tag{44}$$

where $q_e(x,t) = 5\cos[(3\pi/2)(x + (2/3))]$ for the problem A and $q_e(x,t) = 5\cos[(3\pi/2)(x + (2/3))]\sin(2\pi t/t_f)$ for the problem B, respectively. The relation between $q_e(x,t)$ and $\mathbf{q}_e(t)$ is given by Equation (31). We define the following deviation variables:

$$\mathbf{X} \equiv \mathbf{x} - \mathbf{x}_e \tag{45}$$

$$\mathbf{\Sigma} = \mathbf{q} - \mathbf{q}_e \tag{46}$$

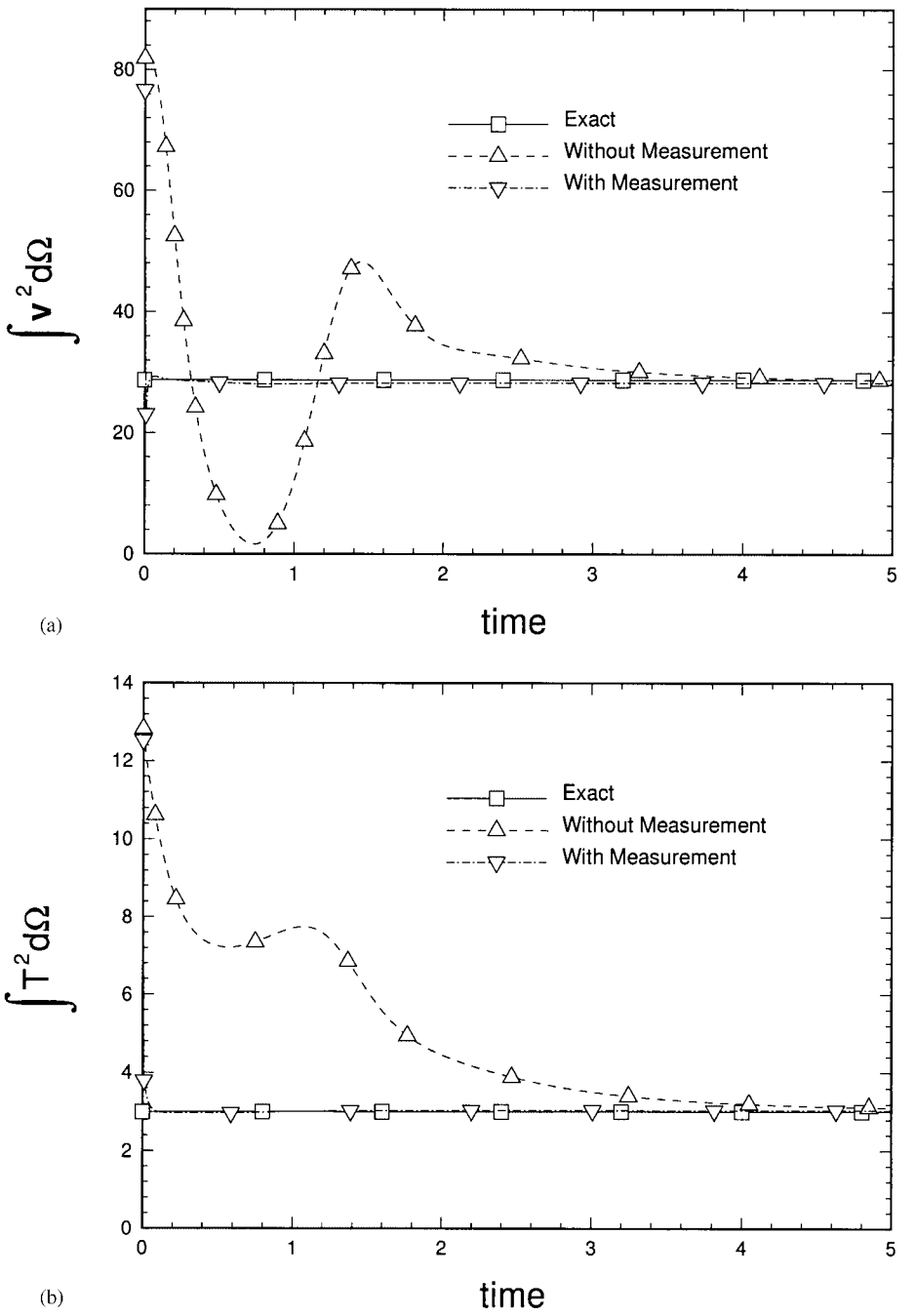

Figure 3. Performance of the Kalman filter for the problem A (3% measurement error).

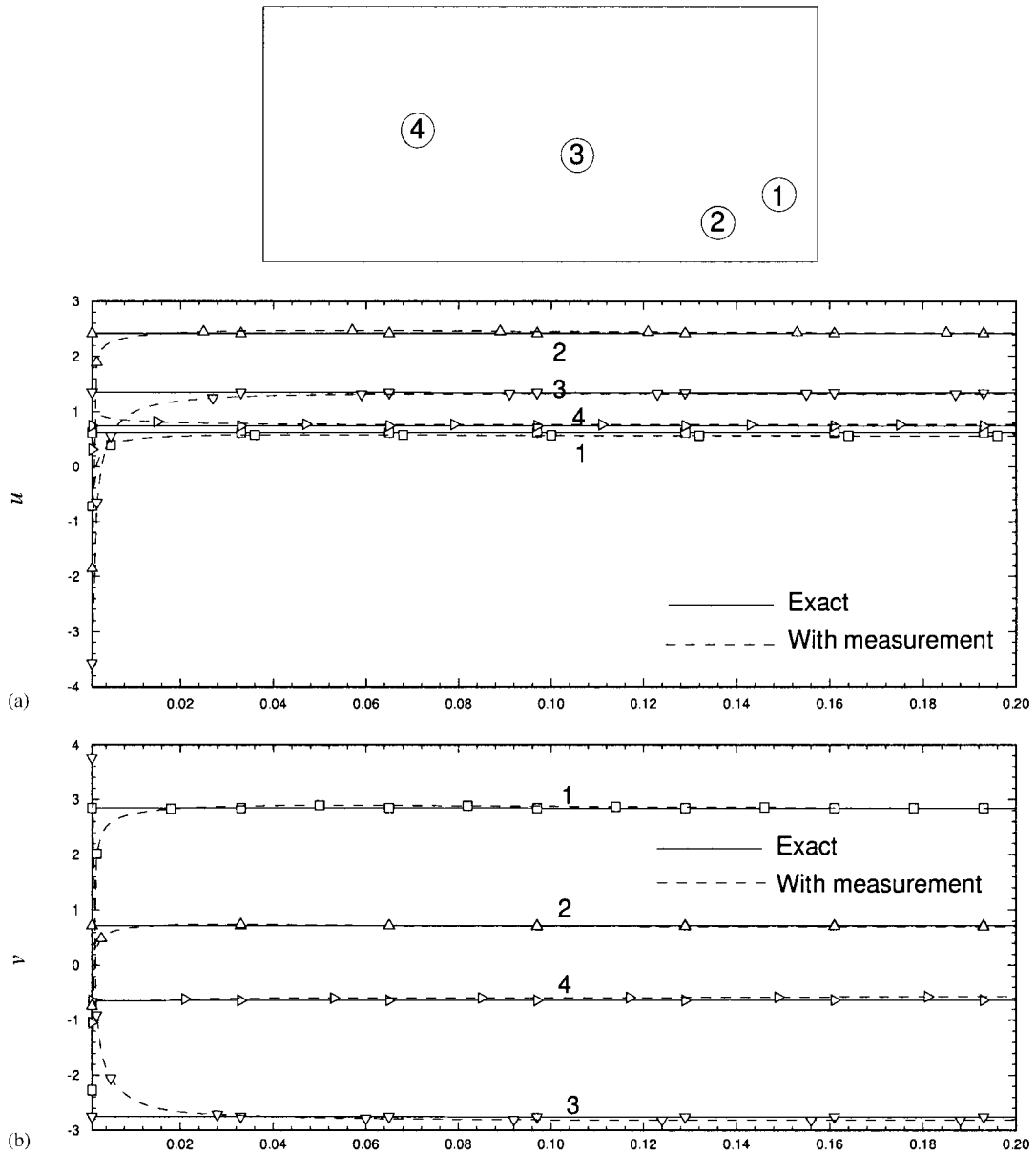

Figure 4. Estimated velocity and temperature from the Kalman filter at selected locations, indicated at the top of the figure, for the problem A (3% measurement error): (a) u, (b) v and (c) T.

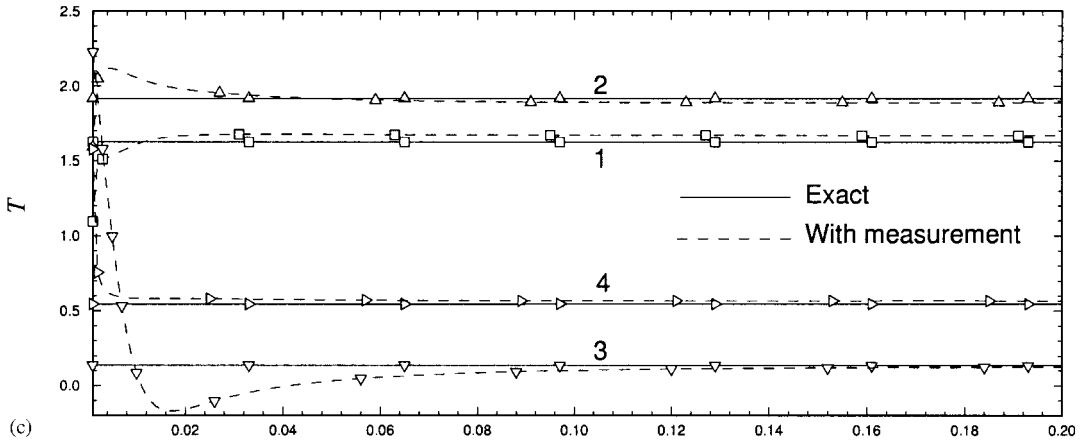

Figure 4. (*Continued*).

where $\mathbf{x}$ is the state vector defined in Equation (26). If we subtract Equation (44) from Equation (25) and linearize the non-linear vector function $\mathbf{f}$ around $\mathbf{x}_e$, we find the following equation:

$$\frac{\mathrm{d}\mathbf{X}}{\mathrm{d}t} = \mathbf{A} \cdot \mathbf{X} + \mathbf{D} \cdot \boldsymbol{\Sigma} \tag{47}$$

$$\mathbf{X}(t=0) = \mathbf{X}^0 \tag{48}$$

where the matrix $\mathbf{A}$ is given by Equation (39) and $\mathbf{X}^0$ is the initial deviation. The performance function defined for the optimal feedback controller, Equation (24), may be rewritten in terms of the deviation variables by exploiting the orthogonality of empirical eigenfunctions as

$$J = \frac{1}{2} \int_0^{t_\mathrm{f}} \mathbf{X}^\mathrm{T} \mathbf{N} \mathbf{X} \, \mathrm{d}t + \frac{\varepsilon}{2} \int_0^{t_\mathrm{f}} \boldsymbol{\Sigma}^2 \, \mathrm{d}t \tag{49}$$

Here, $\mathbf{N}$ is a diagonal matrix defined as

$$\mathbf{N} = \mathrm{diag}(M_1, M_2, \ldots, M_{NM}, \omega_T N_1, \omega_T N_2, \ldots, \omega_T N_{NT}) \tag{50}$$

where M_i and N_i are given by Equation (23). The parameter ε in Equation (49), which indicates the cost for the control action, is set to be 1.0×10^{-6} and the weighting factor $\omega_T = 50.0$ in the present work. The performance function J in Equation (49) is minimized by using a variational method after introducing the adjoint vector $\boldsymbol{\lambda} = (\lambda_1, \lambda_2, \ldots, \lambda_{NM+NT})^\mathrm{T}$ such that

$$J = \frac{1}{2} \int_0^{t_\mathrm{f}} \mathbf{X}^\mathrm{T} \mathbf{N} \mathbf{X} \, \mathrm{d}t + \frac{\varepsilon}{2} \int_0^{t_\mathrm{f}} \boldsymbol{\Sigma}^2 \, \mathrm{d}t - \int_0^{t_\mathrm{f}} \boldsymbol{\lambda} \cdot \left(\frac{\mathrm{d}\mathbf{X}}{\mathrm{d}t} - \mathbf{A} \cdot \mathbf{X} - \mathbf{D} \cdot \boldsymbol{\Sigma} \right) \mathrm{d}t \tag{51}$$

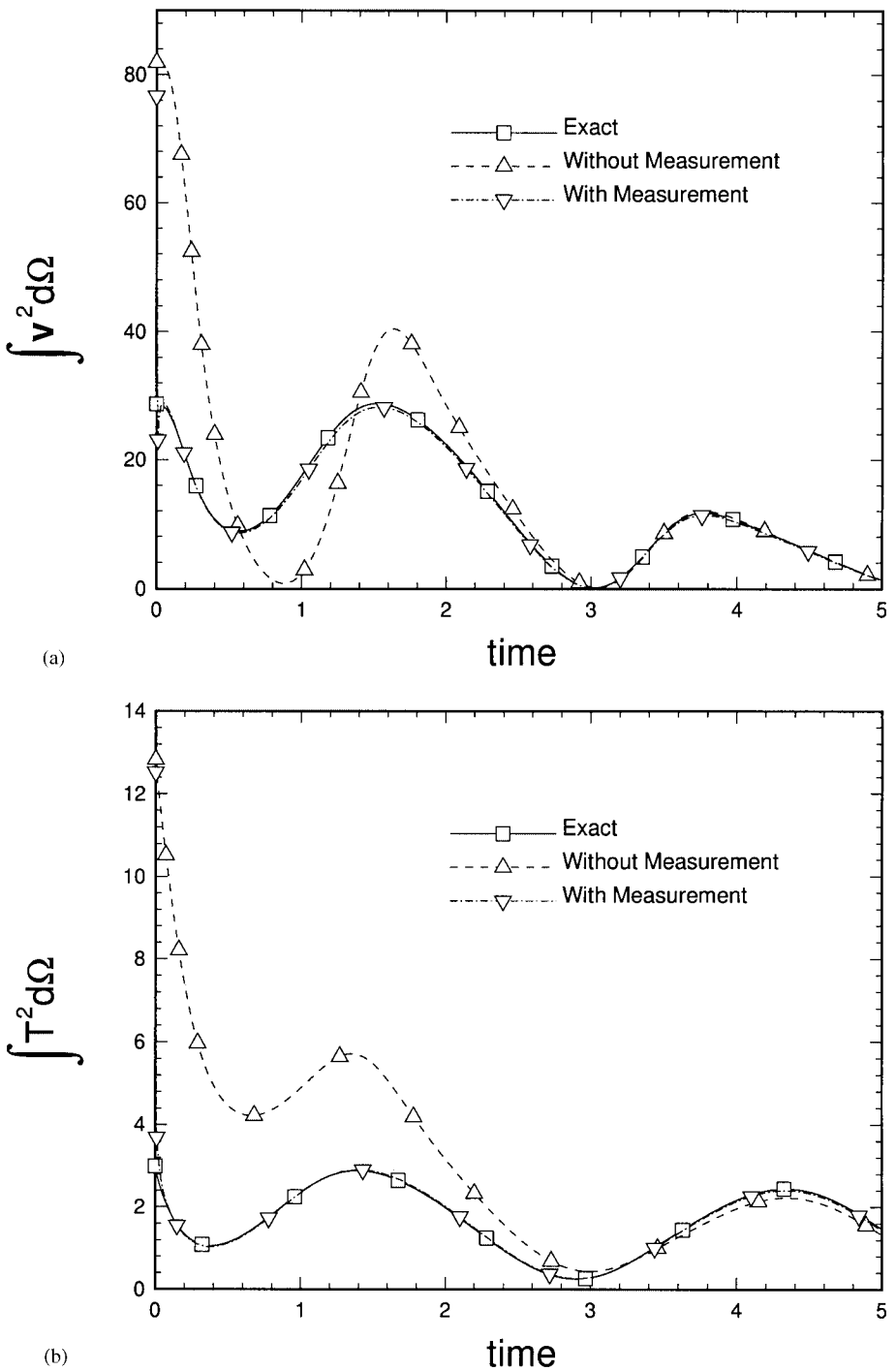

Figure 5. Performance of the Kalman filter for the problem B (3% measurement error).

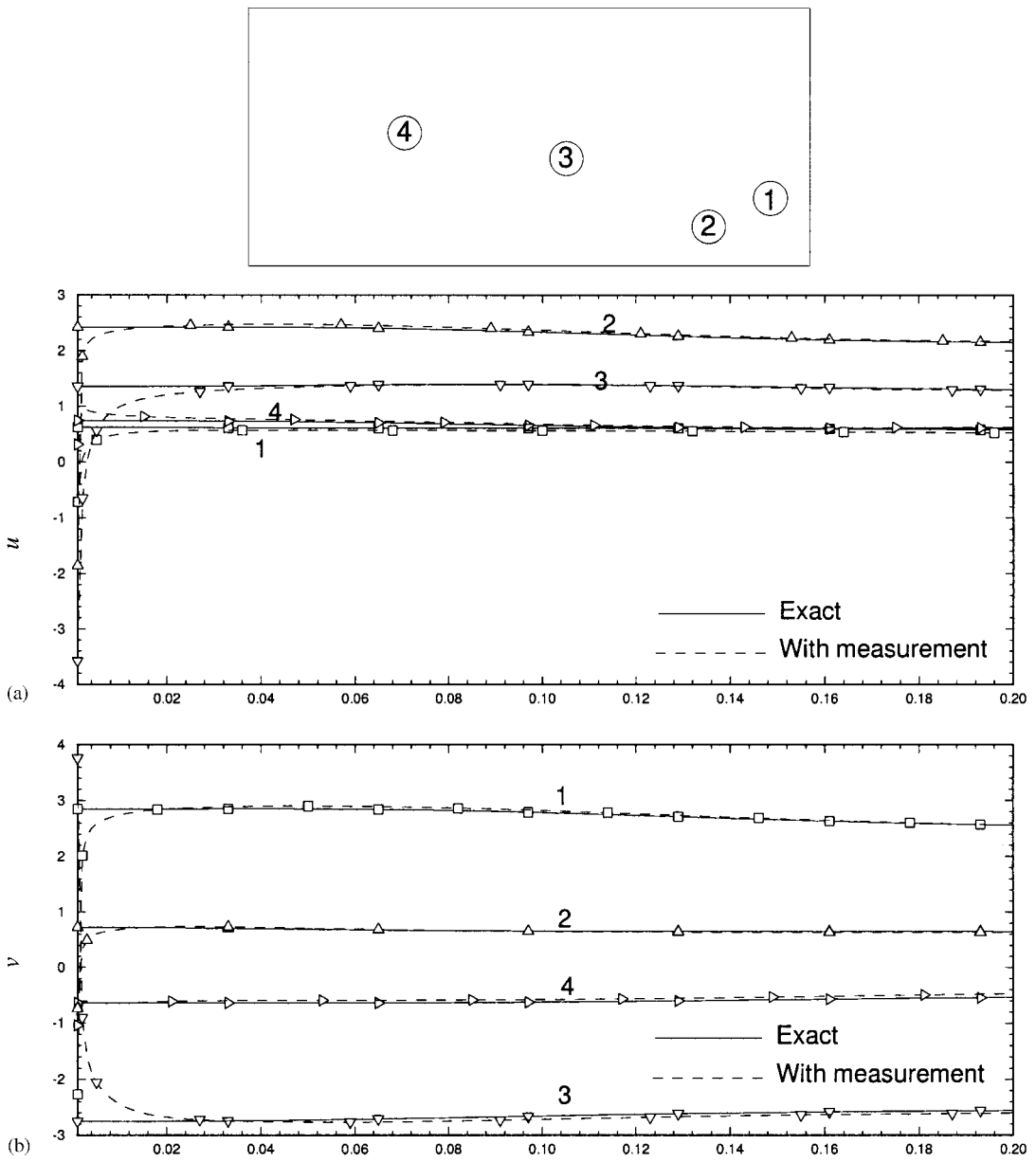

Figure 6. Estimated velocity and temperature from the Kalman filter at selected locations for the problem B (3% measurement error): (a) u, (b) v and (c) T.

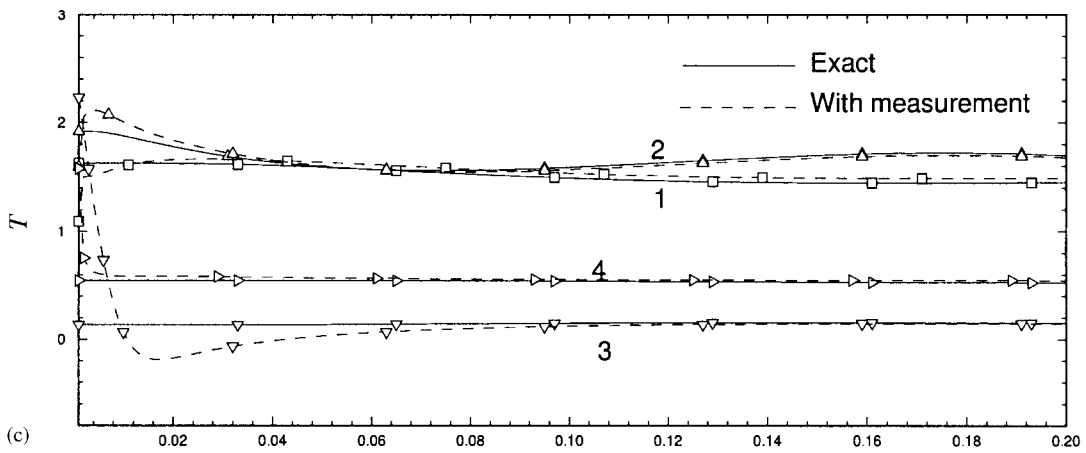

Figure 6. (*Continued*).

Taking a variation of Equation (51) and integrating by parts the variational equation, we find the following set of adjoint equations and an expression for the optimal control:

$$\frac{\mathrm{d}\boldsymbol{\lambda}}{\mathrm{d}t} = -\mathbf{A}^{\mathrm{T}}\boldsymbol{\lambda} - \mathbf{N}^{\mathrm{T}}\mathbf{X} \tag{52}$$

$$\boldsymbol{\lambda}(t = t_{\mathrm{f}}) = 0 \tag{53}$$

$$\boldsymbol{\Sigma} = -\frac{1}{\varepsilon}\,\mathbf{D}^{\mathrm{T}} \cdot \boldsymbol{\lambda} \tag{54}$$

The resulting splitted boundary value problem, Equations (47), (48), (52)–(54), may be solved by introducing the following Riccati transformation:

$$\boldsymbol{\lambda} = \mathbf{S}\mathbf{X} \tag{55}$$

where $\mathbf{S}$ is a matrix. Substituting Equation (55) into Equation (52) and exploiting Equations (47) and (54), we find that the matrix $\mathbf{S}$ satisfies the following equation:

$$\frac{\mathrm{d}\mathbf{S}}{\mathrm{d}t} + \mathbf{S} \cdot \mathbf{A} - \frac{1}{\varepsilon}\,\mathbf{S} \cdot [(\mathbf{D} \cdot \mathbf{D}^{\mathrm{T}}) \cdot \mathbf{S}] + \mathbf{A}^{\mathrm{T}} \cdot \mathbf{S} + \mathbf{N} = 0 \tag{56}$$

$$\mathbf{S}(t = t_{\mathrm{f}}) = 0 \tag{57}$$

Once $\mathbf{S}$ is obtained by solving Equation (56), the optimal control $\boldsymbol{\Sigma}$ is given in terms of the deviational state $\mathbf{X}$ by exploiting Equations (54) and (55) as follows:

$$\boldsymbol{\Sigma} = -\frac{1}{\varepsilon}\,(\mathbf{D}^{\mathrm{T}} \cdot \mathbf{S}) \cdot \mathbf{X} \tag{58}$$

which is the sought optimal feedback controller. In actual implementation, we adopt the steady solution of Equation (56) in Equation (58). Then, the feedback control strategy is quite

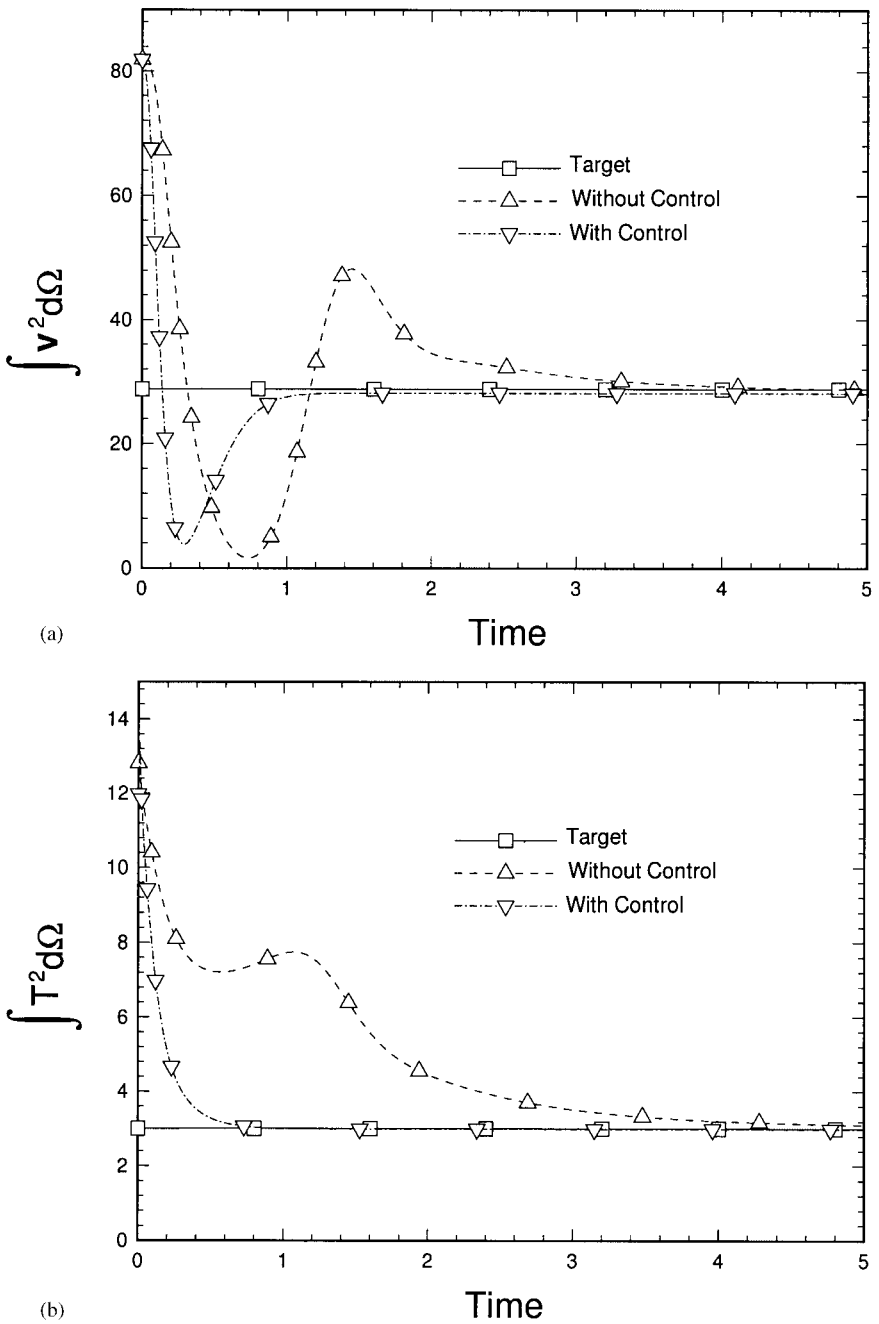

Figure 7. Feedback control with state identification for the problem A, with 3% measurement error. (a) $\int \mathbf{v}^2 \, d\Omega$ and (b) $\int T^2 \, d\Omega$.

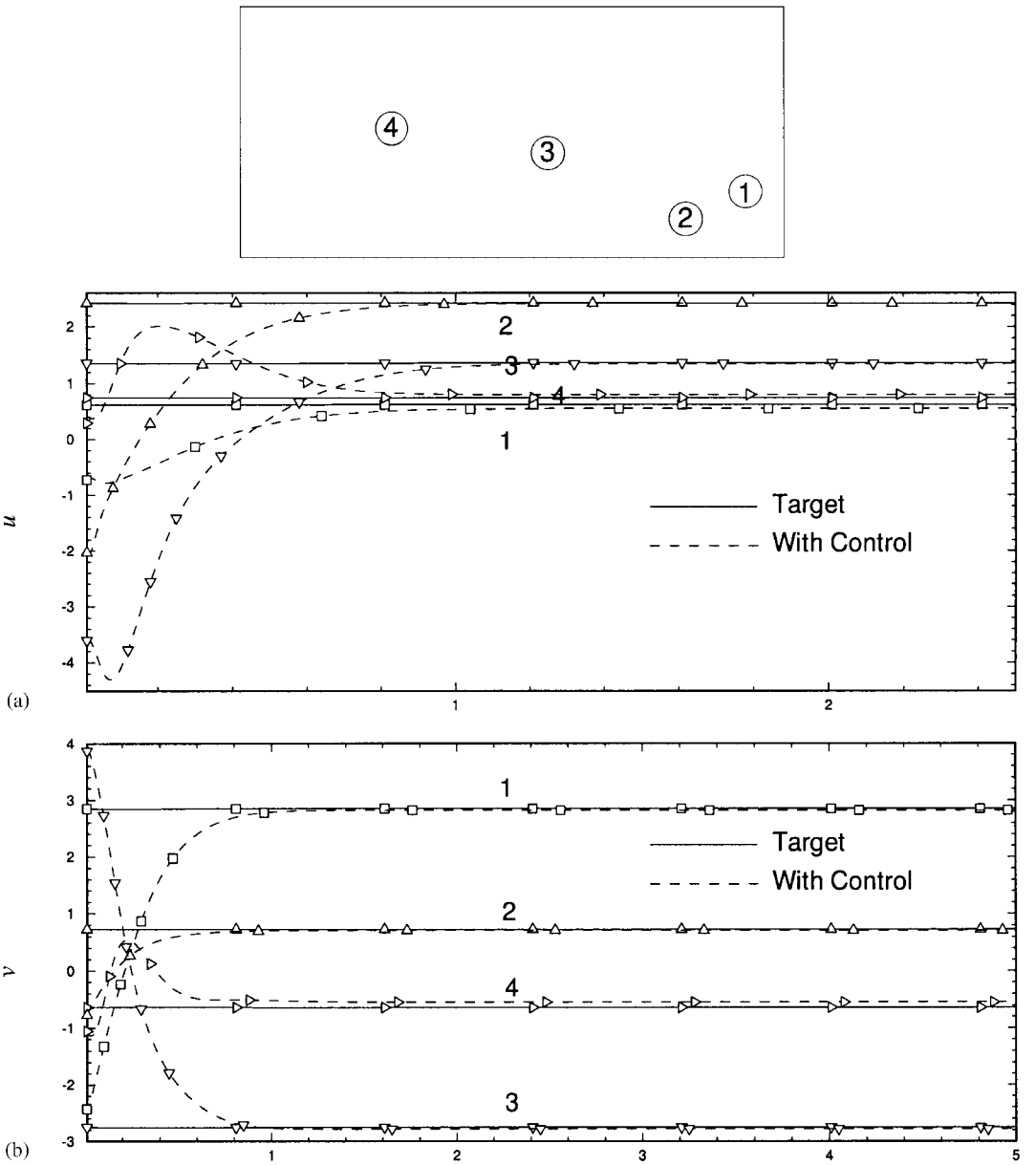

Figure 8. Velocity and temperature trajectories at selected locations for the case of Figure 7: (a) u, (b) v and (c) T.

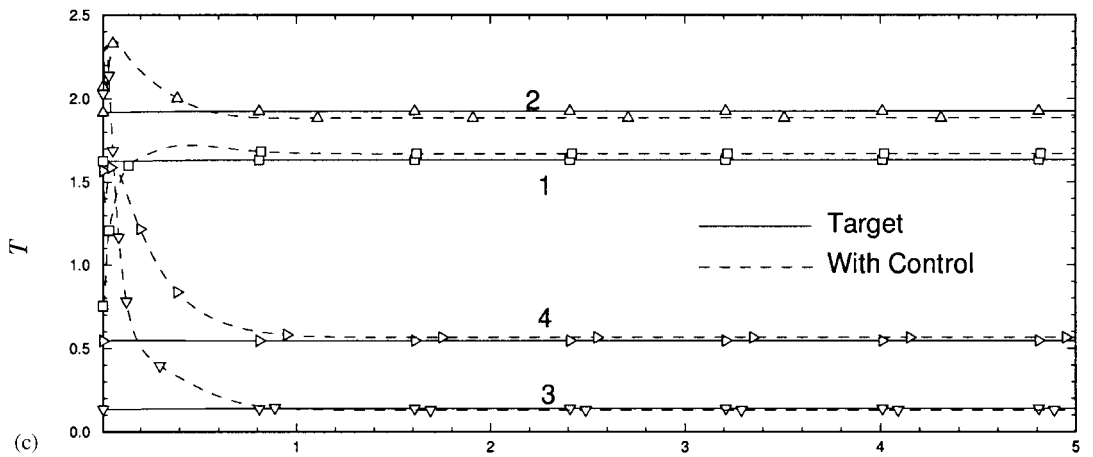

Figure 8. (*Continued*).

straightforward. Once we estimate the velocity and temperature fields in the system domain using measurements, the deviation vector $\mathbf{X}$ is determined by taking the difference between the present state of the system $\mathbf{x}$ and the target state $\mathbf{x}_e$. Since $(\mathbf{D}^{\mathrm{T}} \cdot \mathbf{S})$ in Equation (58) is given *a priori*, the deviation vector $\mathbf{X}$ gives the deviational input $\mathbf{\Sigma}$. The control input $\mathbf{q}$ is then determined by

$$\mathbf{q}(t) = \mathbf{q}_e + \mathbf{\Sigma}(t) \tag{59}$$

Figure 7 shows the performance of the feedback controller for the problem A, when the velocity and temperature are measured at the measurement points shown in Figure 2 with 3% relative measurement error. It is shown that the feedback controller drives the system promptly to the preset velocity and temperature fields. For comparison, the dynamic behaviour of the velocity and temperature fields without feedback control action is also plotted. More detailed information about the performance of the feedback controller can be found in Figure 8(a)–8(c), where the velocity and temperature variations at selected points are plotted for the case of Figure 7. Similar results for the problem B are plotted in Figures 9(a), 9(b) and 10(a)–10(c), where it is demonstrated that the feedback controller enforces the velocity and temperature fields to the desired path in spite of the initial deviation and the 3% relative measurement error.

5. CONCLUSION

An optimal state feedback control is synthesized for the Rayleigh–Bénard convection, that enforces the intensity of convection to a preset constant value or makes it follow a prescribed trajectory promptly regardless of initial deviation or disturbance by exploiting the velocity and temperature measurements at selected locations. The separation principle [3] allows these control problems to be solved by means of the Kalman filtering and the linear quadratic regulator (LQR). However, the straightforward application of these techniques

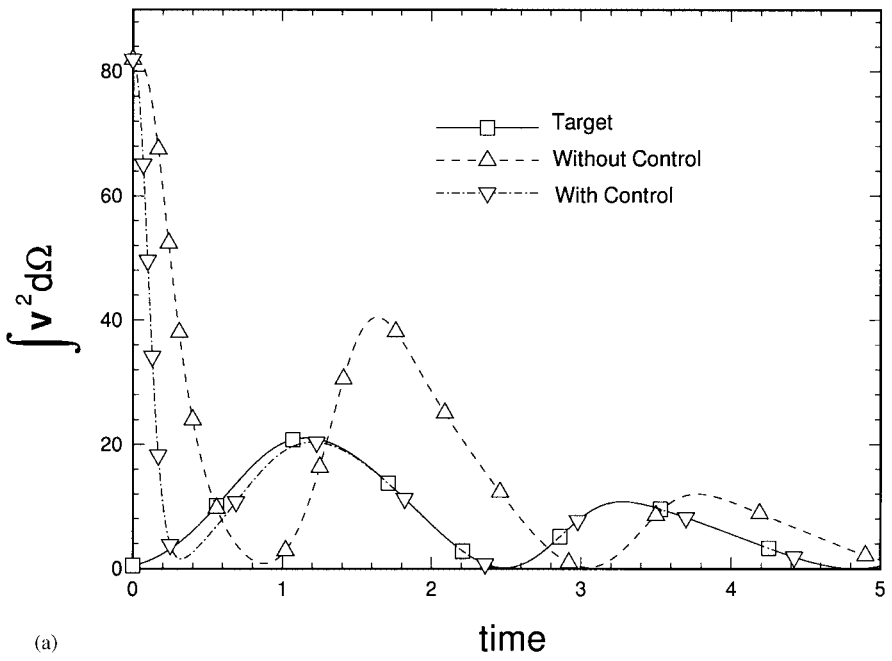

(a)

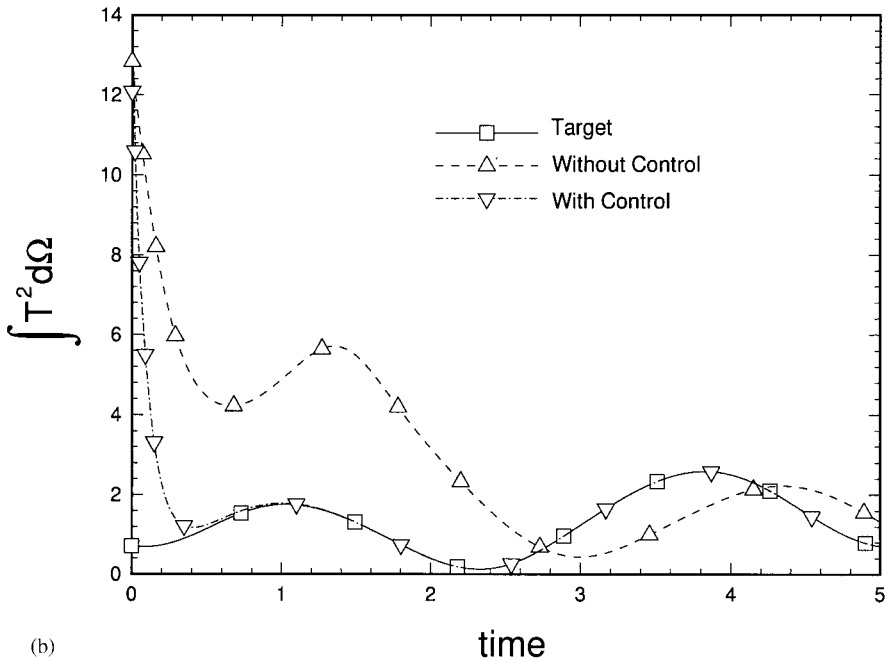

(b)

Figure 9. Feedback control with state identification for the problem B, with 3% measurement error: (a) $\int \mathbf{v}^2 \, d\Omega$ and (b) $\int T^2 \, d\Omega$.

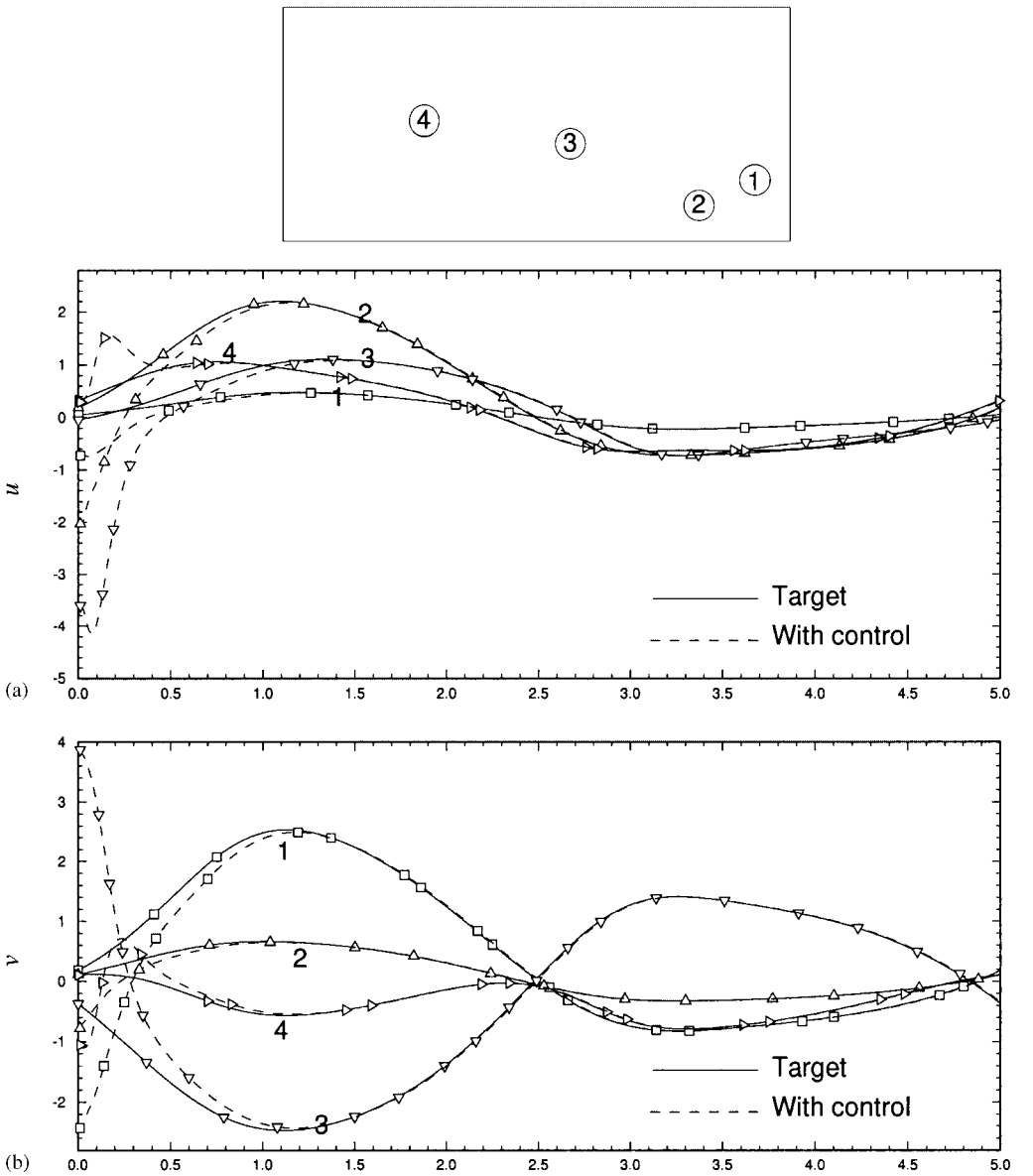

Figure 10. Velocity and temperature trajectories at selected locations for the case of Figure 9: (a) u, (b) v and (c) T.

to the Boussinesq equation is never feasible due to the tremendous amount of computer time and memory required to solve the covariance equations. This difficulty is circumvented in the present investigation by employing the Karhunen–Loève Galerin procedure [5, 6, 8] that reduces the Boussinesq equation to a minimal set of ordinary differential equations. The performance of the state feedback controller and estimator based on this low-dimensional

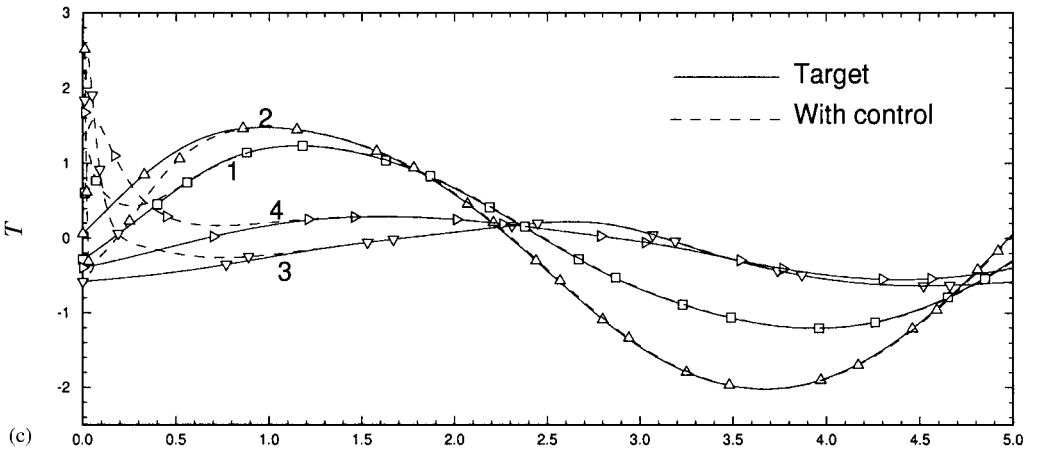

Figure 10. (*Continued*)

dynamic model is assessed with several numerical experiments and is found to yield satisfactory results.

ACKNOWLEDGEMENT

This work is supported by the Applied Science Research Institute of Sogang University.

REFERENCES

1. Chandrasekhar S. *Hydrodynamic and Hydromagnetic Stability*. Oxford University Press: Oxford, 1969.
2. Drazin PG, Reid WH. *Hydrodynamic Stability*. Cambridge University Press: Cambridge, 1981.
3. Anderson BDO, Moore JB. *Optimal Control*: *Linear Quadratic Methods*. Prentice-Hill: Englewood Cliffs, NJ, 1990.
4. Minkler G, Minkler J. *Theory and Application of Kalman Filtering*. Magellan: Palm Bay, FL, 1993.
5. Park HM, Cho DH. Low dimensional modeling of flow reactors. *International Journal of Heat Mass Transfer* 1996; **39**(16):3311–3323.
6. Park HM, Lee MW. An efficient method of solving the Navier–Stokes equation for the flow control. *International Journal for Numerical Methods in Engineering* 1998; **41**:1131–1151.
7. Loève M. *Probability Theory* (4th edn). Springer: New York, 1977.
8. Park HM, Lee MW. Control of Navier–Stokes equations by means of mode reduction. *International Journal for Numerical Methods in Fluids* 2000; **33**:535–557.
9. Park HM, Chung OY. Inverse natural convection problem of estimating wall heat flux. *Chemical Engineering Science* 2000; **55**:2131–2141.
10. Courant R, Hilbert D. *Methods of Mathematical Physics 1*. Wiley-Interscience: New York, 1962.

